Cardiac C-arm CT: Efficient Motion Correction for 4D-FBP

M. Prümmer[1], L. Wigström[2,4], J. Hornegger[1], J. Boese [3], G. Lauritsch [3], N. Strobel [5], R. Fahrig [2]

[1] Institute of Pattern Recognition, FA University Erlangen-Nuremberg. {pruemmer, hornegger}@informatik.uni-erlangen.de

[2] Department of Radiology, Stanford University. {fahrig, larsw }@stanford.edu

[3] Siemens AG, Medical Solutions, Forchheim, Germany. {guenter.lauritsch, jan.boese}@siemens.com

[4] Center for Medical Image Science and Visualization, Linköping University, Sweden

[5] Siemens AG, Medical Solutions, Stanford University. norbert.strobel@siemens.com

Abstract— **Cardiac C-arm CT is a promising technique that enables 3D cardiac image acquisition and real-time fluoroscopy on the same system. The goal is to bring 3D imaging to the interventional suite for improved therapy planning, guidance, and monitoring. For the reconstruction of 3D cardiac image data, a complete set of projections from a specific heart phase is required. One approach to reduce motion blurring caused by the beating heart is to acquire multiple sweeps using the C-arm and retrospectively select the projections that are closest to the desired cardiac phase. In order to further improve the temporal resolution, novel image processing algorithms that utilize retrospective motion correction were investigated in this study. The main focus of this work is to extend the well established FDK algorithm to incorporate motion correction during the back-projection step using a subject specific computed motion field. In a simulation study we show that motion blurring can be decreased significantly using the subjects' individual estimated heart motion based on a time series of retrospectively gated FDK reconstructions. In our experiments using an animal model we investigated the following two scenarios: (I) Can the image quality from a single sweep be improved given a subjects' individual prior computed motion field? (II) Can improved image quality be achieved using the full temporal resolution of a multi-sweep scan for motion estimation in combination with motion correction? Our results show that increasing temporal resolution using an first order estimated 4D motion vector field of the subjects' individual heart motion in the FDK-4D algorithm can decrease motion blurring substantially for both investigated scenarios.**

Index Terms— **Cardiac C-arm CT, heart motion estimation, retrospective motion correction, FDK-4D.**

I. INTRODUCTION

CARDIAC motion presents a significant challenge in cardiac angiography. Cardiac C-arm CT is a new procedure that will combine the advantages of cardiac CT that is used for diagnostic cardiac imaging and C-arm systems that are commonly used during interventions because of their higher flexibility, real-time imaging capability and high spatial resolution for 2D imaging. Novel multi-sweep data acquisition protocols for C-arm CT were introduced by Lauritsch *et. al.* [1] that allow ECG synchronized alternating forward and backward sweeps in order to achieve retrospective gating of the projection data according to a desired cardiac phase (see Figure 1). The challenge is to exclude movement in the reconstruction process as much as possible; only those projections for which motion of the heart is expected to be minimal are used for the reconstruction. Minimal movement occurs in the end diastolic phase which can be detected in the ECG in a relative time window of usually 60-100% between subsequent R-peaks. In C-arm CT, multi segment reconstruction has to be used since a single scan lasts several heart cycles. Current C-arm devices cover an angular range of $\pi + 2\times$ fan-angle for circular short-scan reconstruction, rotating at a constant angular speed (with the exception of acceleration and deceleration at the start and end of a run) in 4-10 seconds depending on the total number of projection images desired. Given the limited scan speed of the C-arm, significant variability in the heart rate during the ECG synchronized sweeps can influence the temporal resolution in a negative manner such that the 3D reconstructed image exhibits motion artifacts and blurring. Therefore novel algorithms to reduce motion blurring in C-arm CT-based cardiac imaging are required.

Methods to reconstruct 3D images of the cardiac anatomy with angiography systems have been investigated previously. A 3D reconstruction framework for coronary arteries using a precomputed 4D motion field was investigated by Blondel *et. al.* [2]. A method to reconstruct moving objects from cone beam X-ray projections acquired during a single rotational run using a given motion vector field was introduced by Schäfer *et. al.* [3]. Schäfer introduced an approximat 4D extension of the FDK algorithm and presented simulation studies using a coronary model where the motion is known. An overview of different concepts used in dynamic CT was published by Bonnet *et. al.* [4]. Bonnet introduced a reconstruction algorithm based on a voxel-specific dynamic evolution compensation. The algorithm provides four-dimensional image sequences with spatio-temporal information, where each frame is reconstructed using a long-scan acquisition mode on several half-turns. Pack and Noo [5] introduced an ART iterative algorithm with a projection and backprojection operator that are matched for dynamic computed tomography with known motion field. They also proposed a method for evaluating the sufficiency of the

This work was supported by Siemens AG, Medical Solutions, Forchheim, Germany, NIH grant R01 EB 003524 and by the Lucas Foundation, HipGraphics, Towson, Maryland, USA [7]), BaCaTec and by Deutsche Forschungsgemeinschaft (DFG), SFB 603, TP C10.

projection data.

In this work we introduce a combined framework of a pure data driven technique to estimate the patients individual 4D heart motion and an extended FDK-like algorithm where the temporal resolution is increased via temporally dependent spatial warping of the filtered backprojections (FBPs) during reconstruction. The goal of this work is the combination of state-of-the-art image based motion registration techniques and reconstruction of images of the beating heart. The introduced framework is optimized for motion estimation and correction of clinical images of the ventricles that are filled with contrast agent via venous injection during data acquisition.

In this paper we first present an image registration technique, optimized for heart motion estimation. We then outline an FDK-like algorithm that allows correction of motion during backprojection based on the estimated heart motion. Results are shown using a simulated heart model and in vivo data from an animal model.

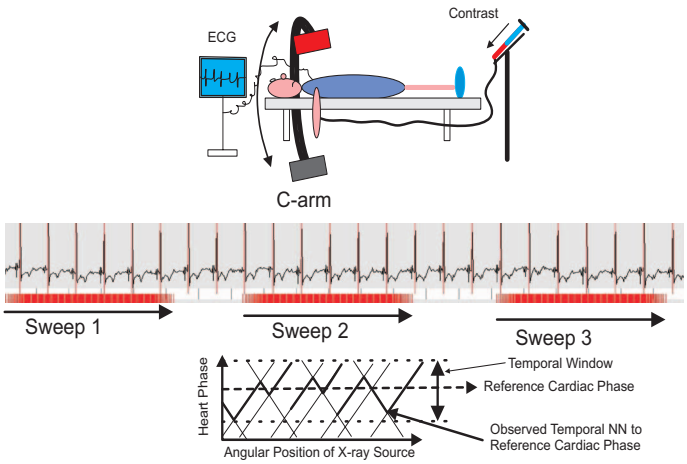

Fig. 1. Acquisition scheme of multi-sweep C-arm scans where contrast is injected during one breathold over all sweeps. The projection data is gated retrospectively according to a reference cardiac phase.

II. METHODS

In the following, we define the cardiac phase that is desired for a motion corrected reconstruction as the *reference cardiac phase* (RCP) $t_r \in [0, 100]$, where the cardiac phase is denoted in percent between a subsequent R-peak. Images that are reconstructed using a standard retrospectively gated FDK (RG-FDK) reconstruction of cardiac phase t_i are denoted by $\boldsymbol{f}_{t_i} \in \mathbb{R}^{N_x \times N_y \times N_z}$. N_s is the number of ECG synchronized C-arm sweeps.

A. Motion Estimation

To reduce motion blurring we first estimate, using a sequence of N_v initial RG-FDK reconstructions $\boldsymbol{f}_{t_i}$, for $i = 1, ..., N_v$ several different cardiac phases, the patients' individual 4D cardiac deformation. The discrete set T contains all cardiac phases $t_i \in T$ of the initial RG-FDK reconstructions. The reconstructed image $\boldsymbol{f}_{t_i}$ is defined on a grid $\boldsymbol{x}_{t_i} \in \mathbb{R}^{N_x \times N_y \times N_z \times 3}$. The estimated individual heart motion provides the basis for retrospective motion correction. In this approach we apply a standard non-rigid 3D-3D registration technique as introduced by Modersitzki *et. al.* [6] to compute the relative 3D deformation $\tilde{\boldsymbol{u}} \in \mathbb{R}^{N_x \times N_y \times N_z \times 3}$ between all image pairs (f_{t_r}, f_{t_i}). We denote

$$\boldsymbol{u}_{t_i} \quad := \quad \tilde{\boldsymbol{u}}_{t_i}(\boldsymbol{x}_{t_r}) \tag{1}$$

as the relative motion vector field (MVF) from cardiac phase t_r to t_i, defined on grid $\boldsymbol{x}_{t_r}$ such that

$$f_{t_r}(\boldsymbol{x}_{t_r}) \quad = \quad f_{t_i}(\boldsymbol{x}_{t_r} - \boldsymbol{u}_{t_i}). \tag{2}$$

Let P be the set that contains all acquired projection images of a multi-sweep scan, then P^t is a subset of P that provides the retrospectively selected projection images of cardiac phase t where for each projection angle one projection image is selected that is closest to the cardiac phase t. P^t_β denotes the β-*th* projection image where the index β is ordered according to an increasing projection angle of a short-scan projection data set P^t. The cardiac phase of a projection image is denoted by $\tau(P^t_\beta)$. The *effective* cardiac phase of a reconstruction using the set of images P^t is

$$\tau_E(t) = \frac{1}{|P^t|} \sum_{\beta=0}^{|P^t|} \tau(P^t_\beta). \tag{3}$$

Due to the acquisition protocol, $\tau_E(t)$ is not a linear function of t. The cardiac phases $T = \{t_1, t_2, ..., t_{N_v}\}$ of the initial reconstructions that are used to estimate the subjects' individual heart motion are selected according to local minimas of the following *mean cardiac phase error function* of t

$$\bar{\tau}_{Err}(t) = \frac{1}{|P^t|} \sum_{\beta=0}^{|P^t|} |t - \tau(P^t_\beta)|. \tag{4}$$

By performing an even number of N_s sweeps, we expect to be able to choose N_s cardiac phases where the RG-FDK reconstructions present only minor motion artifacts, although the expected motion of the heart for a particular cardiac phase should also be considered. All $t_i \in T$ are selected according to local minimas in (4). However, it is not required that the selected RCP, desired for reconstruction, lies in a cardiac phase where only minor motion is expected and (4) provides a local minima. In this case we select for the computation of the MVF another RCP that provides sufficient image quality for motion registration and interpolate afterwards a new MVF that describes the relative heart motion from all other cardiac phases t_i to the desired RCP. The theory of non-rigid reconstruction using variational calculus is well developed, and so we briefly consider some important implementation aspects to improve the result. Here we use a basic curvature-regularized registration algorithm that takes advantage of a fast FFT based solver as described in [6]. In our framework we use a multilevel approach and align each pair (f_{t_r}, f_{t_i}) independently to each other to

avoid error propagation. In general, variational registration approaches that are characterized by an *Euler- Lagrange* equation can be formulated as a system of a non-linear partial differential equations (PDE) that consists of a regularization defined by $\mathcal{A}$ and a force term $\boldsymbol{f}_F$: $\mathcal{A}[\boldsymbol{u}_{t_i}] = \boldsymbol{f}_F(f_{t_r}, f_{t_i}, \boldsymbol{u}_{t_i})$. To solve for $\boldsymbol{u}_{t_i}$ a time marching method [6] is used. Since we deal with mono-modal images we use sum of squared differences (SSD) as distance measure between the image pairs. Solving the PDE for SSD leads to a force term that consists of

$$\boldsymbol{f}_F(\boldsymbol{x}, \boldsymbol{u}_{t_i}) := (f_{t_r}(\boldsymbol{x}) - f_{t_i}(\boldsymbol{x} - \boldsymbol{u}_{t_i}))\nabla_\sigma f_{t_i}(\boldsymbol{x} - \boldsymbol{u}_{t_i}). \quad (5)$$

To deal with contrast and noise problems that arise in (5) during image registration, we apply an additional contrast enhancement for each image pair (f_{t_r}, f_{t_i}). Equation (5) drives the deformation during motion registration and becomes zero if the deformed image $f_{t_i}(\boldsymbol{x} - \boldsymbol{u}_{t_i})$ is identical to the RCP image $f_{t_r}(\boldsymbol{x})$ or if the regularized partial derivative $\nabla_\sigma f_{t_i}(\boldsymbol{x} - \boldsymbol{u}_{t_i})$ becomes zero. Conversely, we observe a strong force term if the partial derivative becomes large especially for high contrast objects. This force term leads to undesirable large forces at dense objects like bones compared to other soft tissue, e.g. the heart. Therefore we define the operator ∇_σ as the convolution of a first derivative of a gaussian kernel G'_σ with standard deviation σ with $f_{t_i}(\boldsymbol{x} - \boldsymbol{u}_{t_i})$ to approximate a smooth partial derivative. Furthermore we equalize the contrast between all soft tissue intensity classes in a manually selected volume of interest (VOI) region around the heart. Using the volume imaging application (*InSpace* (TM), HipGraphics, Towson, Maryland USA [7]) a VOI mask of the heart is created. (5) is then multiplied with the VOI mask such that the forces outside the VOI become zero. To equalize the tissue contrast in each image pair, we create one histrogram from each pair, and then perform histogram equalization using the same intensity transformation for both images. Note that after the transformation the images no longer have real Hounsfield units. A continuous 4D MVF $\boldsymbol{U}(t)$, where

$$\boldsymbol{u}_t \quad = \quad \boldsymbol{U}(t, \boldsymbol{u}_{t_1}, \boldsymbol{u}_{t_2}, ..., \boldsymbol{u}_{t_i}, ...) \quad (6)$$

is obtained by linear or cubic-spline interpolation using all computed $\boldsymbol{u}_{t_i}$ as baseline for the interpolation, where $i = 1, ..., |T|$ with periodic boundary conditions.

B. Reconstruction Method

The reconstruction of dynamic objects using FDK-like algorithms raises two challenges. First, an extended version of the FDK algorithm [8] that can deal with a dynamic geometry according to a moving object $f_{t_i}(\boldsymbol{x}_{t_r} - \boldsymbol{u}_{t_i})$, where $\boldsymbol{u}_{t_i}$ describes the object motion from cardiac phase t_r to another phase t_i, is required. Second, according to the dynamic geometry of the object, the measured Radon data that contributes to each single voxel must be investigated taking into consideration the MVF. The second aspect is important for weighting of redundant Radon data of a short-scan. We introduce in this work an FDK-like algorithm, but do not investigate issues relating to Radon data sufficiency and weighting of redundant data. A similar approach was introduced by Schäfer *et. al.* [3]. We first consider the algorithm introduced in 1984 by Feldkamp [8], Davis [8], and Kress [8] (FDK) and extend the algorithm to 4D, the FDK-4D . This extention allows a 3D motion correction of the FBPs during the FDK-4D reconstruction of a RCP t_r. For a more detailed description of the FDK algorithm we refer to [8], [9]. Our notation of the FDK algorithm is appended to [10]. The FDK reconstruction for planar detectors can be divided into two major steps, where (a, b) denotes a position in the detector plane and the x-ray source moves in the (x, y)-plane along circular trajectories of radius R. First the high-pass ramp-filter $g(a)$ as introduced for parallel-beam geometry and is adapted via coordinate transformation to the cone-beam geometry. The observed projection data $P_\beta^{t_i}(a, b)$ is multiplied by a magnification factor. In a further step the scaled projection data is convolved along each detector row a by the ramp filter:

$$\tilde{P}_\beta^{t_i}(a, b) = \frac{1}{2}(s_\beta(a) P_\beta^{t_i}(a, b) \frac{R}{\sqrt{R^2 + a^2 + b^2}}) * g(a). \quad (7)$$

where $s_\beta(a)$ are standard *Parker* [11] weights. In a further step the filtered projection images are backprojected

$$f_{t_i}^\beta(x, y, z) = \frac{R^2}{W(x, y, \beta)^2} \tilde{P}_\beta^{t_i}(a(x, y, \beta), b(x, y, z, \beta)) \quad (8)$$

where the detector coordinates (a, b) are given as functions depending on $(x, y, z)^\top \in \boldsymbol{x}_{t_r}$ and β with

$$W(x, y, \beta) \quad = \quad R + x\cos(\beta) + y\sin(\beta) \quad (9)$$

$$b(x, y, z, \beta) \quad = \quad z\frac{R}{R - x\sin(\beta) + y\cos(\beta)} \quad (10)$$

$$a(x, y, \beta) \quad = \quad R\frac{-x\sin(\beta) + y\cos(\beta)}{R + x\cos(\beta) + y\sin(\beta)}, \quad (11)$$

where voxel $\boldsymbol{x}_j = (x, y, z)^\top \in \boldsymbol{x}_{t_r}$ denotes the jth voxel in a cartesian grid. For now we assume the simplified case where all projection images are acquired at the same cardiac phase t_r such that

$$\tau(P_\beta^{t_i}) = t_r \qquad \forall\beta \in [0, \pi + \gamma], \quad \forall t_i \in [0, 100], \quad (12)$$

and γ is the overscan angle. Later we will investigate the case where this assumption is not given. The second major step is to integrate, for all voxels in $\boldsymbol{x}_{t_r}$ the filtered backprojections over all projection angles β

$$f_{t_r}(x, y, z) = \int_0^{\pi+\gamma} f_{t_i}^\beta(x, y, z) d\beta \quad (13)$$

to get the reconstructed image of RCP t_r. In an ideal case where assumption (12) holds, (13) simplifies to the FDK algorithm and we can expect a sharp image with no blurring due to motion. In this case the following equation holds

$$|\boldsymbol{u}_{t_i}| \quad = \quad 0 \qquad \forall t_i \in [0, 100]$$

$$f_{t_r}(\boldsymbol{x}) \quad = \quad f_{t_i}(\boldsymbol{x} - \boldsymbol{u}_{t_i}). \quad (14)$$

C. Motion Correction

However, we have to deal with a dynamic object where the dynamic coordinate system for cardiac phase t_i is given by

$$\boldsymbol{x}_{t_i} := \boldsymbol{x}_{t_r} - \boldsymbol{u}_{t_i}, \tag{15}$$

and assumption (14) is not true. First we consider (8) for the case $|\boldsymbol{u}_{t_i}| \neq 0, \quad \forall t_i \in [0, 100] \setminus \{t_r\}$ and a fixed projection angle β where the cardiac phase is given by

$$t^r_\beta := \tau(P^{t_r}_\beta). \tag{16}$$

We evaluate (8) for the cardiac phase t^r_β where the projection image was acquired and the projection geometry therefore describes straight line integrals (rays) for image $f_{t^r_\beta}(\boldsymbol{x}_{t_r})$. Equation (8) is evaluated at all grid positions $(x, y, z)^\top \in \boldsymbol{x}_{t_r}$. The pre-weighting (magnification) and filtering of projection data P^t_β as well as the weighting (de-magnification) during the backprojection can still be applied because we evaluate (8) in the coordinate system where projection data for β is acquired and the rays describe straight lines. Therefore we apply for a single β a standard FBP, but do not accumulate $f^\beta_{t^r_{\beta_i}}(\boldsymbol{x}_{t_r})$ according to (13). To evaluate (13), where the integral for each grid position in $\boldsymbol{x}_{t_r}$ is computed over β, we introduce the deformation of the dynamic object according to (15). The integral in (13) over β can be written as the discrete sum

$$\tilde{f}_{t_r}(\boldsymbol{x}_{t_r}) = \sum_{i=0}^{|P^{t_r}|} f^{\beta_i}_{t^r_{\beta_i}}(\boldsymbol{x}_{t_r} - \boldsymbol{u}_{t^r_{\beta_i}}). \tag{17}$$

of the temporally dependent spatial warped filtered backprojections $f^\beta_{t_i}(\boldsymbol{x}_{t_r} - \boldsymbol{u}_{t^r_\beta})$ according to the MVF. Equation (17) is an approximat scheme for a FBP along curved rays according to the subjects' motion. It allows an efficient implementation scheme, because the additional computation cost during the motion corrected backprojection is the spatial warping using e.g. trilinear interpolation of $f^\beta_{t_i}(\boldsymbol{x}_{t_r} - \boldsymbol{u}_{t^r_\beta})$ according to the MVF. In this work we do not adapt the standard Parker weights $s_\beta(a)$ to the dynamic object geometry according to the MVF. Since a straight ray at cardiac phase t_i can, according to the MVF, describe a curved trace in t_r we suggest a voxel-driven weighting of redundant projection data.

III. SIMULATION STUDIES

A simulation study was performed to investigate for scenario (II) if the temporal resolution can be increased using a subjects' individual estimated MVF in combination with the FDK-4D algorithm. The motion corrected reconstruction is compared to a standard RG-FDK reconstruction. The baseline of a motion artifact free reconstruction is shown in Figure 2 (a) and in the first row of Figure 3.

A. Methods and Materials

Embedded in the FORBILD thorax phantom [12] a dynamic, mathematical model of a beating heart was designed [13]. A volume rendered illustration of the ventricles is shown in Figure 2. Sample slice images of the ground truth are presented in the first row of Figure 3. The 3D motion of the right coronary artery (RCA), left coronary arteries (LCA), and the myocardium are modeled separately. However, there is a link between the motion of the coronaries and the myocardium. For more details see Ref. [13]. The simulated motion mimics the anatomic movement according to clinical data found in the literature [14], [15]. Right coronary arteries have a larger range of motion, while left coronary arteries and myocardium show a significant rest period during the diastolic phase. Figure 2 shows the time dependency of the variables of the motion modeling functions used in this study. A $6 \times 4s$ multi-sweep scan is performed that provides promising image quality in the diastolic phase, but not in the systolic phase, (at 20% of the RR-peak) where the modeled motion is faster (see Figure 2). Reasonable streak artifacts caused by data inconsistencies due to movement affect the image quality. Especially at the phase instances $t = 22.9$ and $t = 56.3$ strong motion occurs during contraction and dilation. The corresponding RG-FDK reconstructed images are so degraded by blurring and strong streak artifacts that any valuable information is difficult to extract.

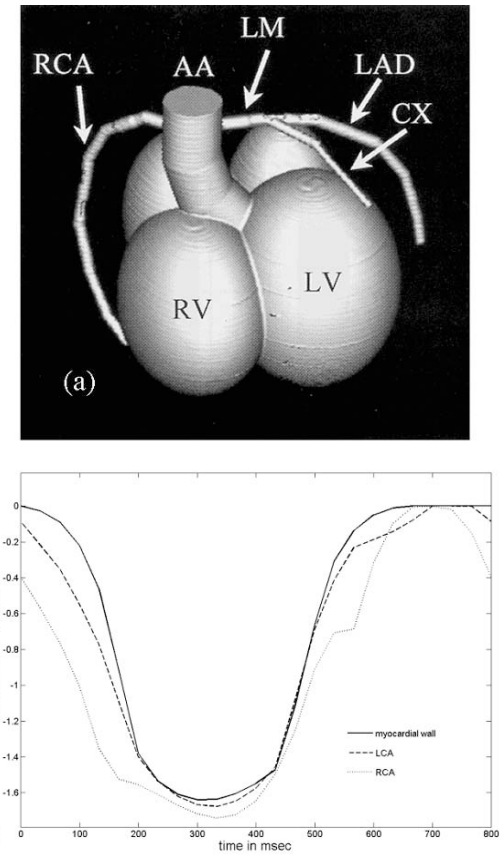

Fig. 2. Volume rendered heart phantom [12] of a dynamic, mathematical model of a beating heart (a). Motion modeling functions used in this study (b). Strong motion is observed around $t = 20$.

B. Results

A retrospective gated FDK reconstruction is shown in the middle row in Figure 3. For the computation of the 4D heart motion five cardiac phases at $t = 14, 29, 49, 88, 94$ were selected, reconstructed using RG-FDK , and used for the motion registration. The reconstructed cardiac phase $t_r = 20$ using FDK-4D is shown in the last row in Figure 3. By comparing the corresponding images of the center and bottom row in Figure 3 it can be seen that temporal resolution can be increased significantly by performing FDK-4D where the subjects' individual heart motion is computed based on multiple RG-FDK reconstructed cardiac phases.

IV. PRECLINICAL STUDIES IN AN ANIMAL MODEL

A. Methods and Materials

The data used in this study was acquired using an in vivo porcine model. Six or four sweeps were acquired in an alternating forward/backward order, each sweep being 4s or 5s duration, with a detector frame rate of 60 frames/s and a resolution of 616×480. The start of each sweep was synchronized to the ECG to achieve an optimal distribution of the projections with respect to the cardiac cycle. For 4s sweeps, 191 projections were acquired per sweep, resulting in a total of 988 projection images for a $6 \times 4s$ scan. For each 5s sweep 247 projections were acquired. Here we discuss some possible clinical scenarios.

(I) Can the image quality from a single sweep be improved given a subjects' individual prior computed motion field?

Here we assume that a pre-intervention reconstructed time series is available from, e.g. clinical CT or a prior 4D acquisition. This can be used to compute the MVF that is later used during a FDK-4D reconstruction of a single-sweep scan during an intervention. We assume a simplified scenario where all image data is acquired at the same point in the respiratory phase. The 6-sweep data reconstructed using conventional retrospective gating provides a baseline temporal resolution (reference) against which the corrected images were compared. Motion estimate was calculated using all 6 sweeps, but for the reconstruction only the first sweep was used.

In scenario (II) we estimate the subjects' individual MVF based on a series of RG-FDK reconstructions and perform a retrospective motion corrected FDK-4D reconstruction using the same projections after application of the temporally dependent spatial warping during backprojection. The goal of (II) is to improved image quality using the full temporal resolution of a multi-sweep scan for motion estimation in combination with motion correction in scenarios where e.g. due to heart beat variations during the scan the expected temporal resolution dropped. Furthermore not all cardiac phases provide a sufficiently short temporal window for a promising RG-FDK reconstruction. Using the FDK-4D algorithm, additional cardiac phases can be reconstructed with an improved temporal resolution. In scenario (II), the data set used for motion estimation, correction and reconstruction uses the full available temporal resolution of a multi-sweep scan. The preclinical studies were performed on an AXIOMArtis dTA C-arm system (Siemens AG,Medical Solutions, Forchheim, Germany).

B. Results

An example of representative image quality in scenario (I) is presented in Figure 4 (bottom row) that showing a motion corrected reconstruction of one single-sweep scan using FDK-4D . The MVF used for the motion correction was computed based on a RG-FDK reconstructed series of a $6 \times 4s$ multi-sweep scan. The reconstruction using standard FDK for the one single-sweep data is shown in Figure 4 (middle row). In the single-sweep case temporal resolution is poor, since no retrospective gating is possible assuming all projections of a short-scan are used for the reconstruction. The top row in Figure 4 shows a standard RG-FDK reconstruction of a $6 \times 4s$ multi-sweep scan that we see as a reference for the image quality compared to the FDK and FDK-4D reconstruction.

Results of scenario (II), where the MVF is estimated based on a $4 \times 4s$ scan that is extracted out of a $6 \times 4s$ scan, are shown in Figure 5. Here Figure 5 (a), a RG-FDK reconstruction of a $6 \times 4s$ scan, is seen as a reference for the RG-FDK and FDK-4D reconstruction (see Figs. 5 (b) and (c)) based on a $4 \times 4s$ scan that is extracted out of the $6 \times 4s$ scan. Another result of scenario (II) is shown in Figure 6. Here (a) and (c) show a standard RG-FDK reconstruction of a $4 \times 5s$ scan for comparison with the corresponding motion corrected FDK-4D reconstruction shown in (b) and (d).

V. CONCLUSIONS AND DISCUSSION

We have shown that increased temporal resolution can be achieved using a first order motion estimation via 3D-3D non-rigid registration applied on a pure RG-FDK reconstructed time series, with correction applied in an FDK-4D algorithm. One of the applications of the FDK-4D algorithm is to retrospectively increase temporal resolution and thus reduce motion blurring in reconstructions where, due to possible heart rate variations during the scan, the expected temporal resolution was not achieved.

For scenario (I) we showed that using a subjects' individual prior estimated 4D motion field, the FDK-4D algorithm is able to decrease motion blurring significantly using data from a single sweep for the reconstruction as shown in Figure 4. For scenario (II) we showed that using the full temporal resolution of a $4 \times 5s$ multi-sweep scan for motion estimation based on a series of RG-FDK reconstructions, combined with retrospective motion correction a significant reduction of motion blurring can be achieved. However, the reduction of motion blurring is constrained by the accuracy of the MVF which again is an approximation of the subjects's individual heart motion and based on the provided image quality of the RG-FDK reconstructed time series.

In conclusion, increasing temporal resolution using an estimated 4D MVF of the subjects' individual heart motion in the FDK-4D algorithm can decrease motion blurring and improve image quality. We showed that retrospective motion

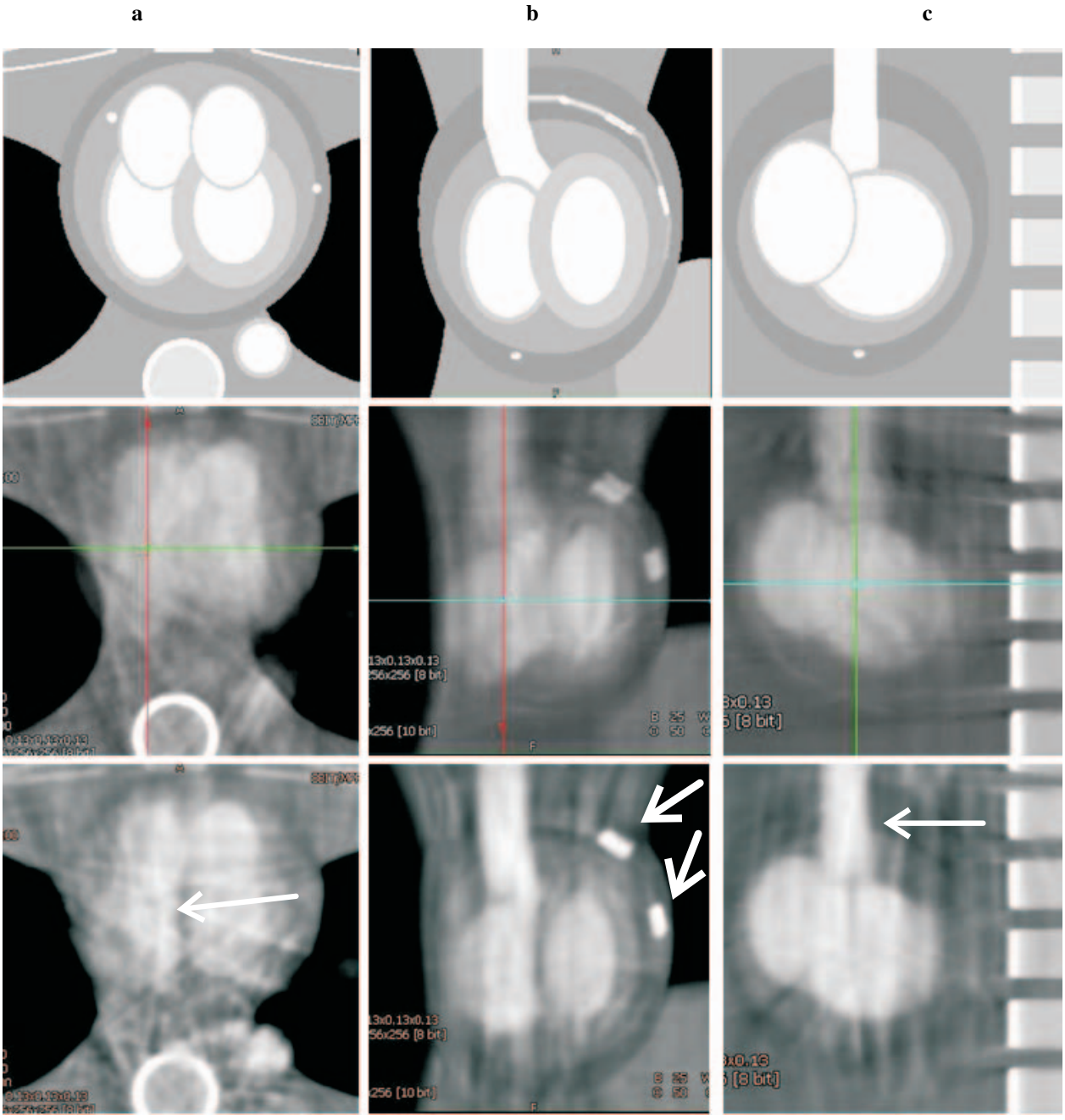

Fig. 3. Results from the simulations using the FORBILD phantom. The ground truth $t = 22$ is shown in the upper row and a conventional retrospectively gated FDK reconstruction (RG-FDK) based on $6 \times 4s$ simulated sweeps in the middle row. The selected reference cardiac phase $t_r = 20$ corresponds to rapid systolic contraction and the images consequently exhibit severe motion artifacts and blurring. A motion corrected reconstruction using the proposed FDK-4D is shown in the bottom row. The motion vector field (MVF) was estimated based on five RG-FDK reconstructed cardiac phases. Compared to the RG-FDK the result shows less blurring, and the ventricular walls can be more accurately localized and delineated. The left column shows a transversal multiplanar reformation (MPR), the middle column a coronal and the right column a sagittal MPR, respectively.

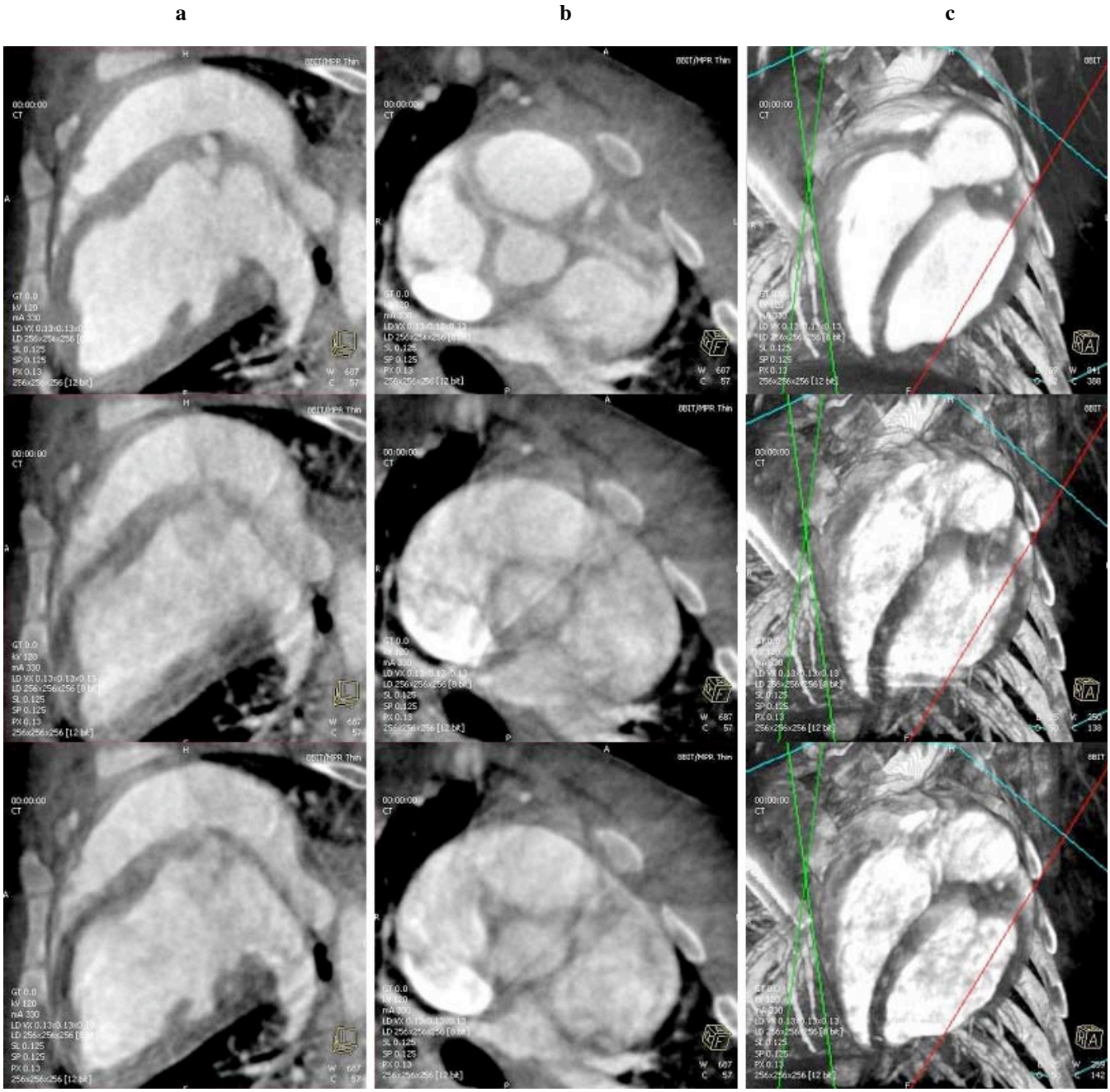

Fig. 4. SCENARIO (I) - Cardiac RG-FDK reconstruction from a $6 \times 4s$ sweep acquisition ($t_r = 75$) (top row). This provides a reference temporal resolution against which a standard FDK reconstruction using 191 projections without gating (middle row) and a motion corrected reconstruction (FDK-4D) without gating (bottom row) were compared. The left column shows a long axis MPR view, the middle column a short axis view at an atrial level, and the right column a volume rendering with a cut plane applied through the left and right ventricles. The pigs' individual MVF was computed based on ten RG-FDK reconstructions.

Fig. 5. SCENARIO (II) - Retrospectively gated reconstruction (RG-FDK) using 191 projections from a $6 \times 4s$ multi-sweep scan (a). This is considered the gold standard for (b) and (c), which are based on $4 \times 4s$ sweeps extracted from the $6 \times 4s$ scan. (b) shows a standard RG-FDK reconstruction and (c) the proposed FDK-4D reconstruction. The motion vector field (MVF) used for the motion correction in (c) is estimated based on a series of RG-FDK reconstructed images from the extracted $4 \times 4s$ scan. A long axis MPR view at $t_r = 35$ is shown.

correction is a promising technique that is applicable to a variety of clinical applications. One possible future application of retrospective motion correction is improvement of SNR by including additional corrected and resampled projections from temporal windows outside of the targeted reconstruction phase.

REFERENCES

[1] G. Lauritsch, J. Boese, L. Wigström, H. Kemeth, R. Fahrig, "*Towards Cardiac C-arm Computed Tomography*", IEEE Transactions on Medical Imaging, vol. 25, pp. 922-934, 2006.

[2] C. Blondel, R. Vaillant, G. Malandain and N. Ayache, "*3D tomographic reconstruction of coronary arteries using a precomputed 4D motion field*", Phys. Med. Biol. Vol. 49, pp 2197-2208, 2004.

[3] D. Schäfer , J. Borgert, V. Rasche, and M. Grass "*Motion-Compensated and Gated Cone Beam Filtered Back-Projection for 3-D Rotational X-Ray Angiography*", IEEE TRANSACTIONS ON MEDICAL IMAGING, VOL. 25, NO. 7, pp. 898-906, JULY 2006.

[4] S. Bonnet, A. Koenig, S. Roux, P. Hugonnard, R. Guillemaud and P. Grangeat, "*Dynamic X-ray computed tomography*", Proc. IEEE, vol. 91, no. 10, pp. 1574-1587, Oct. 2003.

[5] J. D. Pack and F. Noo, "*Dynamic computed tomography with known motion field*", Proc. SPIE Vol. 5370, p. 2097-2104, Medical Imaging 2004.

[6] J. Modersitzki, "*Numerical Methods for Image Registration*", Oxford University Press, 2004.

[7] *InSpace* 2006, http://www.insideinspace.com, Sept. 2006.

[8] L.A. Feldkamp, L.C. Davies, and J.W. Kress, "*Practical cone-beam algorithm*", J. Opt. Soc. Am., vol. A1, pp. 612-619, 1984.

[9] H. Turbell, "*Cone-Beam Reconstruction Using Filtered Backprojection*", Linköping University, Sweden, 2001, Diss. 672, ISBN 91-7219-919-9.

[10] Buzug, "*Einführung in die Computertomographie*", Springer Verlag Heidelberg, ISBN 3-540-20808-9, 2004.

[11] D. L. Parker, "*Optimal short scan convolution reconstruction for fanbeam CT*", Med. Phys. 9(2), pp. 254-257 ,April 1982.

[12] http://www.imp.uni-erlangen.de/forbild/english/results/thorax/thorax.htm.

[13] A. Hölzel "*Dynamisches Herzmodell für die Computertomographie (CT) und Anwendungen für die CT-Herzbildgebung*", Master thesis, Fachhochschule Anhalt, Köthen, Germany, December 5, 2002.

[14] S. Achenbach, D. Ropers, J. Holle, G. Muschiol, W. G. Daniel, and W. Moshage: "*In-Plane Coronary Arterial Motion Velocity: Measurement with Electron-Beam CT*", Radiology, vol. 216, pp. 457-463, 2000.

[15] Y. Wang, E. Vidan, and G. Bergman, "*Cardiac Motion of Coronary Arteries: Variability in the Rest Period and Implications for Coronary MR Angiography*", Radiology, vol. 213, pp. 751-758, 1999.

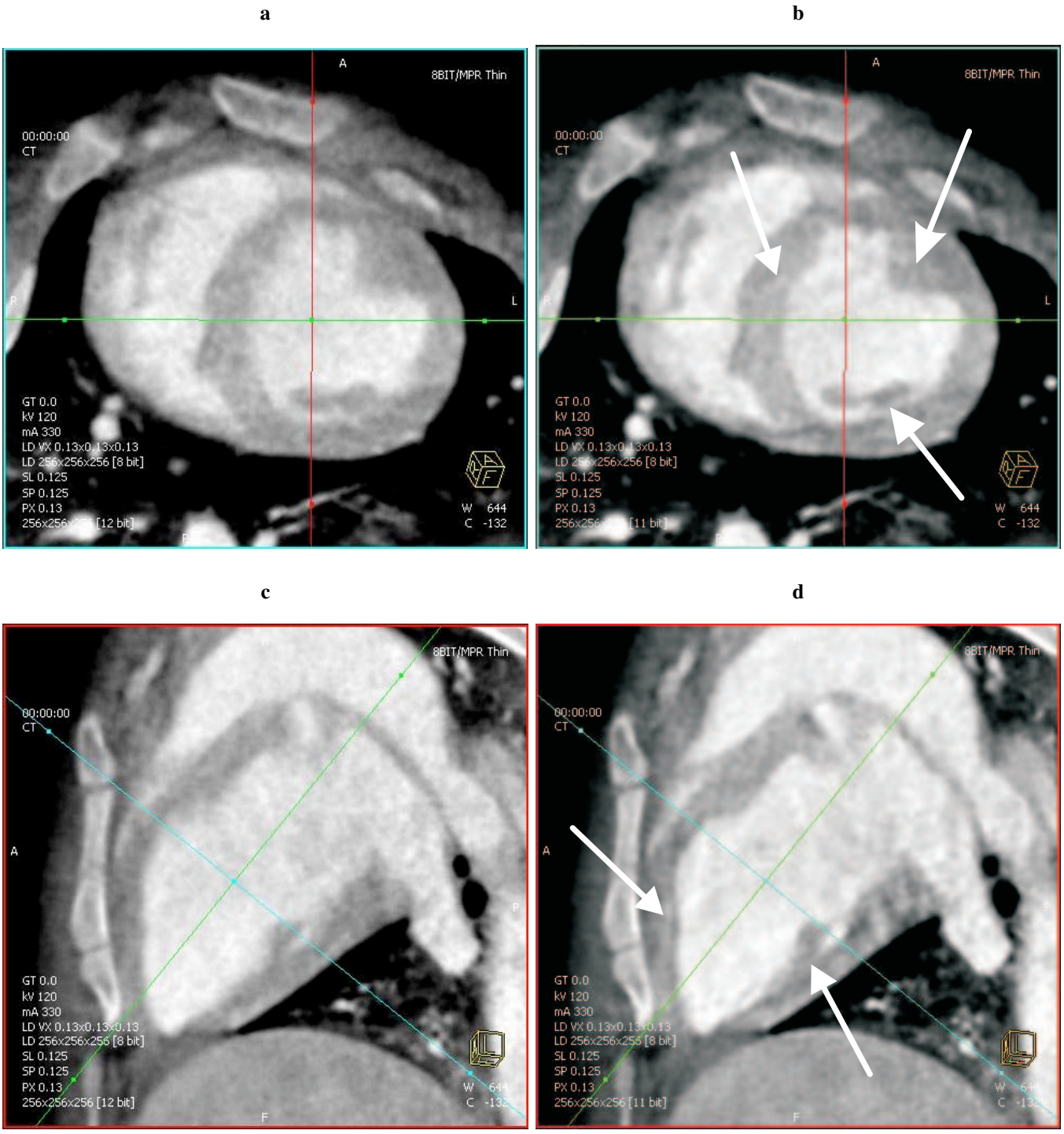

Fig. 6. SCENARIO (II) - A comparison between RG-FDK (a) and the motion corrected FDK-4D reconstruction (b) in a short axis MPR view ($t_r = 28$). Projection data were acquired using $4 \times 5s$ sweeps, and the MVF was estimated based on a series of RG-FDK reconstructions. (c) and (d) show the corresponding comparison in a long axis MPR view. The motion corrected reconstruction (b and d) demonstrates reduced blurring compared to (a and c).